PARAMETERS CONTROLLING THE THERMAL FATIGUE PROPERTIES OF CONVENTIONALLY-CAST AND DIRECTIONALLY-SOLIDIFIED TURBINE ALLOYS

G. R. Leverant, T. E. Strangman, and B. S. Langer

Materials Engineering and Research Laboratories
Pratt & Whitney Aircraft, East Hartford, Connecticut 06108

ABSTRACT

Thermal-mechanical fatigue tests were performed on conventionally-cast and directionally-solidified nickel-base superalloys to identify the key parameters controlling the thermal fatigue properties of gas turbine components. It was found that crack initiation has a strong tendency to occur in the surface coating applied to these alloys for oxidation and hot corrosion (sulfidation) resistance. Crack initiation in the coating is a function of the coating mechanical properties, the thermal strain range (including the thermal expansion mismatch strains generated between the coating and superalloy substrate), and the strain-temperature cycle phase relationship. The rate of crack propagation in the superalloy substrate depends on the strain intensity factor range, the alloy elastic constants, and the phase relationship between strain and temperature.

Over the past five years an intensive effort has been underway at Pratt and Whitney Aircraft to define the key material and cycle variables responsible for turbine airfoil degradation by thermal fatigue cracking and to develop quantitative approaches for predicting component thermal fatigue lifetimes based on identification of these variables. The approach has been based on the development of a specimen design and testing method that can simulate the various strain-temperature phase relationships experienced in turbine airfoils. It has considered, in detail, the role of oxidation-resistant protective coatings on fatigue crack initiation as well as on propagation of coating-initiated cracks into the superalloy substrate. In addition, it has included direct measurement of crack propagation rates in directionally-solidified (D.S.) and conventionally-cast (C.C.) superalloys and the influence of strain-temperature phasing on these propagation rates. With this crack initiation and propagation data, new guidelines have been established for turbine airfoil design for optimum thermal fatigue resistance.

Three γ' [$Ni_3Al(Ti)$] precipitation hardened nickel-base superalloys were included in this study. These were D.S. Mar-M200+Hf (Ni-9.6Co-8.5Cr-12W-4.9Al-2.0Ti-2.2Hf-0.9Cb-0.11C-0.014B), C.C. B-1900+Hf (Ni-9.8Co-8.0Cr-5.9Mo-4.1Ta-6.0Al-1.0Ti-1.2Hf-0.13C-0.013B), and C.C. NX-188 (Ni-18Mo-8Al-0.04C). In addition, both conventional diffusion aluminide and electron beam vapor deposited (overlay) coatings were evaluated.

All thermal-mechanical fatigue (TMF) tests were performed in strain control on tubular specimens with a 1" (2.54 cm) uniform section gage length in closed loop testing machines (1-3). Axial strain was measured with a calibrated L.V.D.T. and its associated extensometry (coaxial quartz tubes) which rested on ridges machined on the inside diameter of the specimen gage section. Temperature was controlled and measured with the aid of a calibrated infrared temperature comparator and both the strain and temperature signals were independently controlled by the closed loop servohydraulic systems. To produce the desired strain-temperature histories, the temperature excursions were obtained by induction heating and forced convective cooling of the outside specimen surface. Total cycle time was 2 1/4 minutes (0.445 cpm, 0.0074 HZ) with a symmetrical cycle shape maintained for the heating and cooling portions of the cycle.

The strain-temperature phase relationships used in the testing of the thin-walled tubes are defined in Figure 1. As indicated in this figure, cycle I has the peak tensile strain at low temperatures and the peak compressive strain at high temperatures. Cycle II is the exact reverse of cycle I, whereas cycle III has both the peak tensile and compressive strains peak at intermediate temperatures with zero strain at the minimum and maximum temperatures.

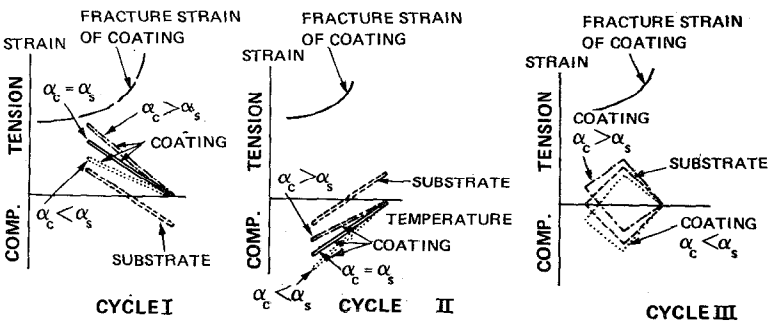

Figure 1. Schematic showing representative thermal-mechanical fatigue cycles in the substrate and coating.

I. Crack Initiation

Thermally-induced strains are generally largest at the surface of an airfoil. As a consequence, thermal fatigue crack initiation in nickel-base superalloy blade and vane airfoils has a strong tendency to occur in 2-5 mil thick coatings that are applied to the surfaces of components to enhance oxidation and hot corrosion (sulfidation) resistance. On occasion, crack initiation will occur intergranularly in the superalloy substrate, itself, but this is not often observed in advanced, hollow airfoil designs. For this reason, this section will concentrate on the properties of coatings and coating/substrate combinations that control fatigue crack initiation.

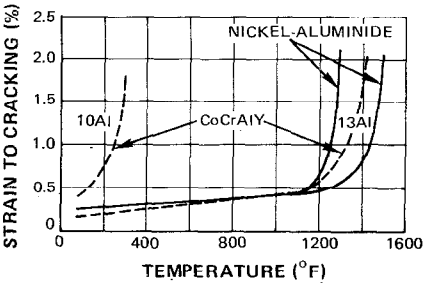

Figure 2. Ductility of CoCrAlY overlay and diffusion nickel-aluminide coatings.

A. Basic Considerations

Both overlay electron beam vapor deposited NiCoCrAlY and diffusion aluminide coatings exhibit a characteristic ductile-to-brittle transition temperature. The transition temperature is relatively high (1250-1450°F) for diffusion aluminide coatings and insensitive to chemistry (aluminum content) over practical limits as shown in Figure 2. NiCoCrAlY overlay coatings can provide more desirable lower brittle-to-ductile transition temperatures (around room temperature) which are very responsive to chemistry alterations, principally chromium and aluminum. Alteration in the aluminum content of the overlay coatings has the largest single effect upon coating ductility, with the lower aluminum compositions exhibiting the higher ductility. An example of the range of coating ductility behavior which may be achieved with CoCrAlY coatings is also shown in Figure 2. The microstructure of the 13%Al CoCrAlY coating contains a large volume fraction of the β phase (CoAl intermetallic), which is relatively brittle at the lower temperatures. The higher ductility 10%Al CoCrAlY coating is obtained by lowering the aluminum and chromium contents to obtain a coating microstructure which contains a smaller volume fraction of β phase particles dispersed in a ductile γ (cobalt solid solution) matrix. Similar ductility behavior can also be obtained with NiCrAlY and NiCoCrAlY coatings by adjusting compositions. However, decreasing the aluminum and chromium contents also decreases the oxidation/hot corrosion life of NiCoCrAlY coatings. Thus, unlike the diffusion aluminides, the overlay coatings can be adjusted through chemistry selection to provide the best trade-off of oxidation/hot corrosion life and ductility to meet the needs of a given application.

Inspection of Figure 1 indicates that the thermal fatigue behavior of a coated superalloy should be strongly influenced by the strain-temperature cycle shape (cycle I, II or III) as well as the coating ductility. The results of a series of experiments to evaluate this hypothesis are included in Figure 3, where data for coated and uncoated D.S. Mar-M200+Hf tested parallel to the grain growth direction are summarized.* Several major conclusions may be drawn from these results. First, coatings reduce the number of cycles to crack initiation and failure, particularly for cycle I where the tensile strains peak in the range of lower coating ductility. (For C.C. superalloys, coatings can be beneficial for specific cycle shapes because oxidized grain boundaries are sources of crack initiation.) Secondly, cycle shape has a significant effect on cycles to coating crack initiation, with cycle I loading resulting in much earlier cracking. Third, coating composition also has a significant effect on crack initiation. The specimen coated with the more ductile 10%Al CoCrAlY had

*Note that the high strain range of 0.6% was used for experimental expediency. Actual thermal strain ranges generally range from 0.1 to 0.3%, where the cycles to coating crack initiation may be a significant fraction of the component thermal fatigue life.

double the life of the specimen coated with the relatively brittle 13%Al CoCrAlY In fact, the crack that led to failure initiated in the 13%Al CoCrAlY on the specimen coated on the O.D. with that coating, but in the I.D. aluminide coating on the specimen coated on the O.D. with the more ductile 10% CoCrAlY overlay coating.

A more detailed thermal fatigue evaluation has been conducted with ductile NiCoCrAlY overlay coatings on various superalloys. These results will be discussed in the next section.

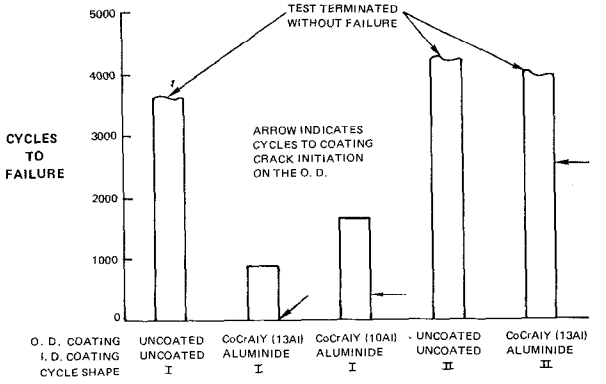

Figure 3. The effect of cycle shape and coating chemistry on TMF of D.S. Mar-M200+Hf (800-1700°F, $\Delta\varepsilon$=0.6%).

B. Detailed Analysis of Crack Initiation in NiCoCrAlY Coated Superalloys

An investigation of the mechanical properties of overlay coatings has shown that, at high temperatures, the flow stress (creep resistance) of ductile NiCoCrAlY coatings is extremely low and significant creep can occur at very low stresses (4). As a result, stress relaxation occurs in the coating at high temperatures during take-off and cruise conditions, and equilibration of the coating to a zero elastic strain condition occurs. It is, therefore, necessary to define the zero elastic strain condition of the coating at the maximum temperature for the three TMF cycles as shown in Figure 1. Schematic coating fracture strain (ductility) curves are also included in this figure. It can readily be observed that the cycle I condition, which has the tensile strain in the coating peaking at low temperatures, where coating ductility can be relatively low, is of primary concern from a coating initiation standpoint. Tensile mean strains in the coating also tend to favor coating cracking under cycle I conditions.

Because the coating and superalloy substrate will, in general, have different coefficients of thermal expansion, α, significant thermal expansion mismatch strains can develop in a coating/alloy system during thermal cycling. These tensile or compressive thermal expansion mismatch strains can, respectively, increase or decrease the magnitude of the coating strain as shown in Figure 1. On the basis of these considerations, cycle I conditions have been used to characterize the thermal fatigue behavior of NiCoCrAlY coatings with limited data being obtained for the other cycle shapes. This choice of cycle shape is also consistent with engine experience; i.e., when thermal fatigue cracking is observed in component airfoils, the location of the cracking is frequently associated with cycle I type thermal strains.

Analogous to structural alloys (5,6) coatings also contain flaws which may contribute to crack initiation when the strain range is sufficiently large. More specifically, coating crack initiation tends to occur preferentially at through thickness flaws (pits and flakes) when they are present (Figure 4). The formation of these defects is discussed in a separate paper (7).

In order to characterize initiation and propagation of coating cracks from coating defects, surface condition of the coating was documented with plastic replicas prior to and during testing. Examination of the sequence of replicas permitted the length of coating cracks to be correlated with the number of cycles. Graphical representation of the surface length of a coating crack as

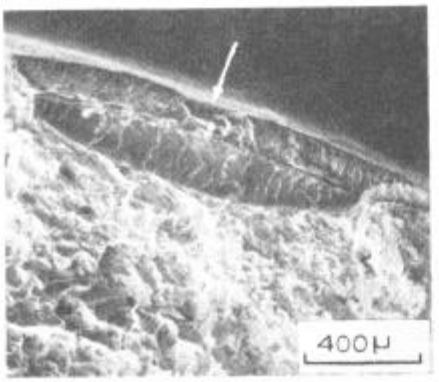

Figure 4. Crack initiation at an overlay coating defect on D.S. Mar-M200+Hf (cycle I, 800-1900°F).

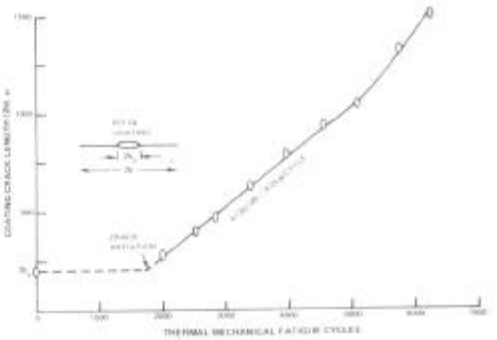

Figure 5. Surface propagation of cycle I [(800-1900°F); $\Delta\varepsilon_{TM}$=0.25%]TMF crack in NiCoCrAlY coating on D.S. Mar-M200+Hf substrate.

a function of the number of TMF cycles for a crack in a NiCoCrAlY coating is shown in Figure 5. The significant features of this graph are the number of cycles required to transform a coating flaw into a fatigue crack (initiation), a constant crack growth rate period, and finally, a period of increasing crack growth rate. Fractographic analysis of coating cracks in various stages of development have shown that substrate crack initiation tends to be approximately concurrent with coating crack initiation. Thus, the thermal fatigue crack is propagating into the substrate while it is propagating at a constant rate in the plane of the coating.

Cycle I, II and III (800-1900°F) TMF coating crack initiation data for 4 mil thick NiCoCrAlY coatings on NX-188, D.S. Mar-M200+Hf, and B-1900+Hf are plotted as a function of the mechanical strain range, $\Delta\varepsilon_{TM}$, in Figure 6. Two important factors controlling crack initiation emerge from this graph. First, as previously discussed, crack initiation occurs significantly faster in cycle I compared to cycles II and III. This results from differences in mean strain in the coating and the temperature dependence of coating ductility (see Figure 1). In addition, while the data for D.S. Mar-M200+Hf and B-1900+Hf fall in the same scatterband, the data for NX-188 is significantly lower. Replotting the cycle I data as a function of $\Delta\varepsilon_{TM}+\Delta\varepsilon_{\alpha}$, where $\Delta\varepsilon_{\alpha}$ is the coating substrate thermal expansion mismatch strain range component, results in convergence of the data for all three substrate alloys into a single scatterband, Figure 7. ($\Delta\varepsilon_{\alpha}$ is ~0.18%, ~0.18%, and ~0.29% for D.S. Mar-M200+Hf, B-1900+Hf, and NX-188, respectively.) This demonstrates the importance of coating/substrate thermal expansion mismatch on thermal fatigue coating crack initiation.

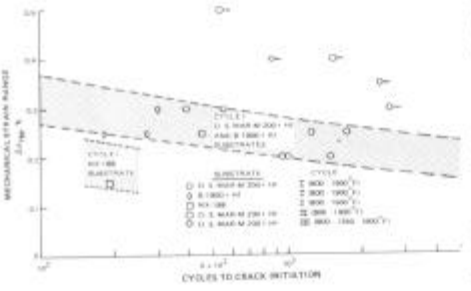

Figure 6. TMF crack initiation in a NiCoCrAlY coating on various superalloy substrates.

While this discussion has dealt exclusively with NiCoCrAlY coatings, it should be noted that similar thermal fatigue behavior has been observed with other coating systems. Furthermore, it has been observed that coating crack initiation trends observed in cyclic burner rig tests are in qualitative agreement with the crack initiation life predictions which were derived from the thermal-mechanical fatigue tests (8).

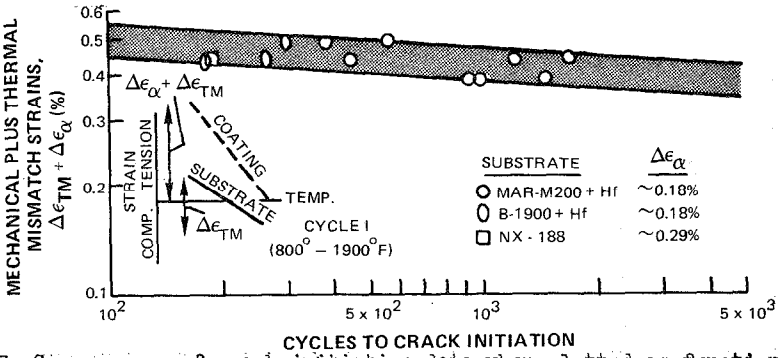

Figure 7. Convergence of crack initiation data when plotted as function of the summation of the mechanical strain and the thermal mismatch strain.

C. Coating Crack Propagation into the Substrate

It has been experimentally demonstrated (see Section II) for through-cracks that the thermal fatigue crack propagation rate, da/dn, for various superalloys, including D.S. Mar-M200+Hf and B-1900+Hf, is dependent on the strain intensity factor range, ΔK_{ϵ}.* However, when surface coating cracks propagate into a superalloy substrate, additional considerations are important. These include the redistribution of load carried by the uncracked coating to the tip region of a surface-connected substrate crack as well as the contribution of $\Delta\epsilon_{\alpha}$ to substrate crack propagation (da/dn).

For cycle I conditions, it can be shown (9) that the magnitude of the elastic thermal expansion mismatch strain between the coating and substrate alters ΔK_{ϵ} and thus da/dn. For a small surface connected substrate crack, the strain (stress) intensity factor range is predominantly a function of the coating thickness (t), $\Delta\epsilon_{\alpha}$ and $\Delta\epsilon_{TM}$. As the crack grows, the mechanical strain term eventually becomes dominant. Since the majority of a component's life is spent when the cracks are small, the thermal expansion mismatch term can substantially affect the life of the component. Therefore, appropriate da/dn vs. ΔK_{ϵ} data for a superalloy substrate can be used in conjunction with coating data and the transient thermal strain analysis for the critical location to calculate the number of cycles to propagate a thermal fatigue crack from an initial flaw size (e.g., the coating thickness) to a critical depth into the component. The important parameters controlling substrate crack propagation rates are discussed in the next section.

II. Crack Propagation

A. Effect of Cycle Shape and Temperature

Thermal-mechanical fatigue crack propagation rates (da/dn) were determined for both conventionally-cast (C.C.) B-1900+Hf and directionally-solidified (D.S.) Mar-M200+Hf as a function of cycle shape and peak cycle temperature. These results are summarized in Figures 8 and 9. In contrast to the results of cycle shape on coating crack initiation, where cracking occurs much more readily in

*The strain intensity range, ΔK_{ϵ}, is utilized for convenience because thermal fatigue is a strain-controlled process. It is defined as $\Delta K_{\epsilon} = \Delta\epsilon\sqrt{\pi a}\, f(g)$ where $\Delta\epsilon$ is the strain range, a the half-crack length, and f (g) the usual geometrical factors. As will be seen in later discussions, the stress intensity range is still considered to be the prime driving force for crack propagation.

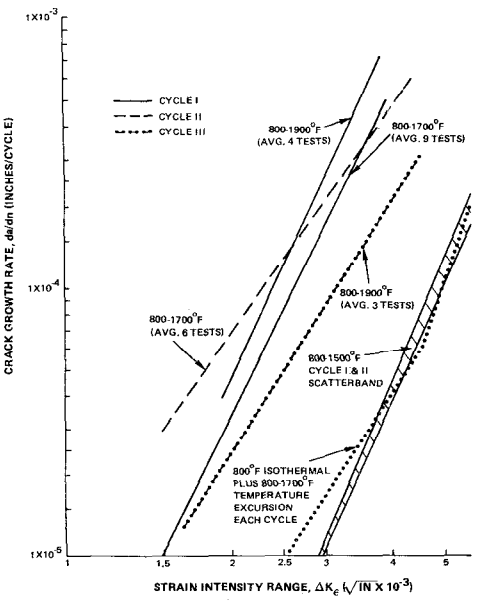

Figure 8. The effect of cycle shape and maximum cycle temperature on TMF crack propagation rate in D.S. Mar-M200+Hf.

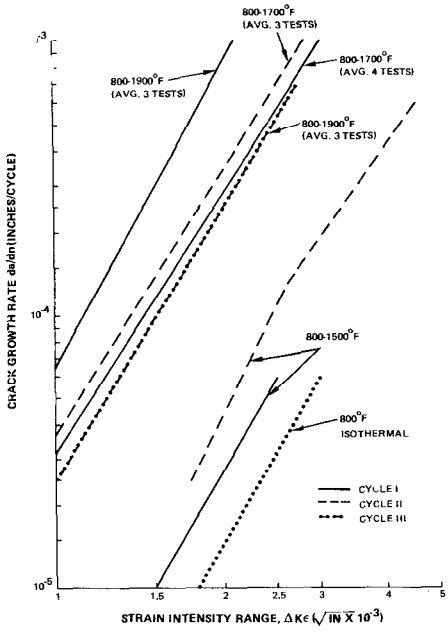

Figure 9. The effect of cycle shape and maximum cycle temperature on TMF crack propagation rate in C.C. B-1900+Hf.

cycle I (Section I), da/dn for cycles I and II in both superalloys is comparable, and, in fact, the average rate is higher for cycle II. For cycle III (peak tensile and compressive strains midway between the temperature extremes), da/dn for both alloys is reduced compared to the results for cycle I and II. Isothermal testing in the low temperature regime (e.g., 800°F) of the thermal fatigue cycle also results in considerably lower da/dn, Figure 9. Increase in peak cycle temperature results in an increase of crack growth rate for both the C.C. and D.S. alloys. Examples for cycle I loading are shown in Figures 8 and 9.

The increase in da/dn with peak cycle temperature (T_{max}) indicates that application of strain at the high temperature is crucial in determining thermal fatigue crack growth rates. The sign of the applied strain at high temperature (tensile or compressive) is relatively unimportant, as shown by the comparable cycle I and II results for a given T_{max}. In addition, comparison of cycle III with cycle I and II results shows that application of strain at T_{max} is more important than simply attaining T_{max} during cycling. This was also shown in an experiment where the D.S. alloy was strained in tension and compression at 800°F and then heated to T_{max} (1700°F) for the completion of each cycle. The crack growth rate (da/dn) for these conditions was markedly lower than da/dn for either cycle I or II loading, Figure 8.

All of these results can be interpreted in terms of the effective ΔK acting at the tip of the crack. A schematic illustration of this concept is shown in Figure 10, and it is based on the fact that creep processes are negligible below about 1550°F for high strength, cast nickel-base superalloys. For example for low temperature (800°F) isothermal loading the crack tip is essentially closed during the compressive half of the cycle, as has been demonstrated in previous studies of low temperature fatigue crack growth in various alloys (10, 11). Therefore, the effective ΔK (ΔK_{eff}) for crack growth is one-half of the range of ΔK, i.e., the tensile-half only.

Where either tensile or compressive strain is applied at $T_{max} \gtrsim 1550°F$, however, stress relaxation can occur at the crack tip (the remainder of the structure or specimen experiences elastic loading) due to thermally-activated plastic deformation (creep). For example, in cycle I loading, stress relaxation at peak strain at T_{max} would result in the crack opening at, say, point A in Figure 10(b) upon reversal of the sign of the strain. This results in a considerably higher ΔK_{eff} for cycle I loading compared to low temperature isothermal loading. A higher ΔK_{eff} results in a larger crack opening displacement ($COD \cong \Delta K_{eff}/4E\sigma_{yield}$, and since, da/dn is proportional to COD (12), a higher crack growth rate. Note, however, that when T_{max} is a relatively low temperature, e.g., 1500°F, stress relaxation is limited and da/dn is comparable to growth rates measured in low temperature isothermal cycling.

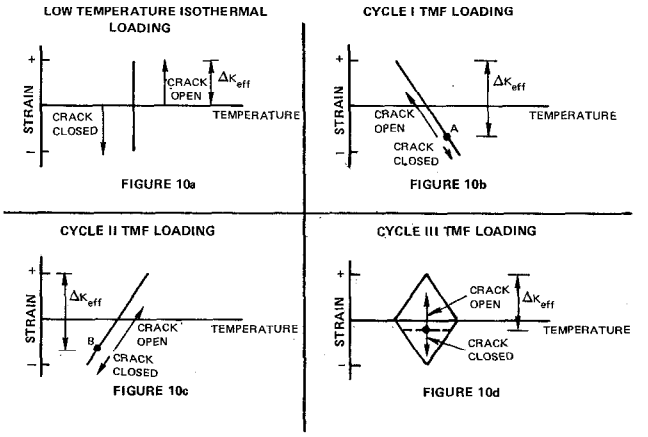

Figure 10. Schematic shows the effect of strain temperature cycle shape on ΔK_{eff} for crack propagation.

Similar agruments can be used to account for cycle II and cycle III results as well (Figures 10(c) and (d)). For cycle II loading creep in tension at T_{max} wedges the crack tip open such that crack closure does not occur until a compressive strain, such as that indicated by point B, is reached. ΔK_{eff} for cycle II is then comparable to that obtained in cycle I. In the case of cycle III loading, the absence of maximum tensile or compressive strains at T_{max} reduces the amount of stress relaxation compared to cycles I and II. Therefore, although ΔK_{eff} is larger than one-half the ΔK range, it is lower than ΔK_{eff} for cycles I and II, and da/dn is reduced.

B. Conventionally-Cast vs. Directionally-Solidified Alloys

Comparison of da/dn for C.C. B-1900+Hf and D.S. Mar-M200+Hf shows that the D.S. alloy is markedly superior in its resistance to thermal fatigue crack propagation, Figures 8 and 9. This is a general result and is found for all testing conditions independent of the specific crack propagation path for each alloy (crack propagation paths are summarized in Table I).

The superiority of the D.S. alloy is directly related to its lower elastic modulus (E) in the growth direction compared to the modulus for C.C. alloys. The magnitude of these elastic moduli are summarized in Table II, from which it is clear that E for the D.S. alloy is lower by 30-40% over the entire temperature range. This indicates that the stress range experienced by the D.S. alloy in TMF cycling is 30-40% lower than that for the C.C. alloy under identical testing conditions. With da/dn proportional to the stress intensity range (2), the markedly lower stresses for the D.S. alloy result in major improvements in resistance to thermal fatigue crack propagation.

This conclusion can, of course, be extrapolated to actual components where thermally-induced stresses are given by $\Delta\sigma = \alpha E \Delta T$, where α is the thermal expansion coefficient (essentially equivalent for the C.C. and D.S. alloys) and ΔT is the temperature gradient. With $\Delta\sigma$ directly proportional to E, the stress range and da/dn are considerably reduced for D.S. turbine blades and vanes.

C. Dependence of the Fatigue Crack Propagation Rate on the Angle Between the Loading Axis and the Grain Growth Direction for D.S. Alloys

Cycle I (800-1900°F) crack growth rates have been measured for D.S. Mar-M200+Hf for various angles (θ) between the grain growth direction and the loading axis. Tests were performed for θ values of 0, 15, 30, 45 and 90°. These data have been discussed in considerable detail elsewhere (2), so this discussion will be limited to the key points emanating from that work.

The slowest crack growth rates were obtained for the longitudinal material (θ=0°) and the most rapid crack growth rates for 45° off-axis tests, Figure 11. The 15° off-axis crack growth rates were 25 to 80% faster than the average 0° growth rates. The 30° and 90° off-axis crack growth rates fell within the same scatterband and were faster than the 15° off-axis test. The crack growth rates for the 45° orientation were similar to those obtained for conventionally-cast B-1900+Hf under identifical test conditions and were about a factor of eight faster than those for the longitudinal material (θ=0°).

Comparison of the crack growth rates as a function of θ with the respective elastic moduli, which are listed in Table II, indicates a relationship similar to that discussed in the previous section in comparing D.S. and C.C. alloys; that is, the higher the elastic modulus, the higher da/dn for comparable loading conditions. In fact, by using the elastic moduli as normalization factors, data for all orientations can be reasonably predicted from the test of a single orientation, Figure 11. As described previously, higher elastic modulus is associated with higher thermal stresses and vice versa such that the driving force for crack propagation (the stress intensity range) is proportional to a power function of E. This approach can also be used to demonstrate that the relative crack growth rates are consistent with the relative crack-opening-displacements at the crack tip (2).

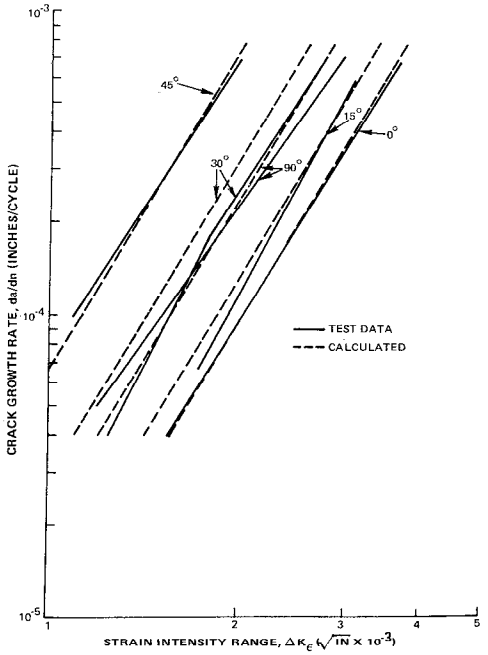

Figure 11. The dependence of fatigue crack propagations rate on the angle between the grain growth direction and the loading axis for D.S. Mar-M200+Hf.

Table I

Crack Propagation Paths for C.C. B-1900+Hf and D.S. Mar-M200+Hf

	Temperature Range °F		
	800-1500	800-1700	800-1900
D.S. Mar-M200+Hf			
Cycle I	TG	TG	TG
Cycle II	TG	TG	--
Cycle III	--	--	TG
C.C. B-1900+Hf			
Cycle I	TG	90% TG 10% IG	50% TG 50% IG
Cycle II	TG	10% TG 90% IG	--
Cycle III	--	--	50% TG 50% IG

TG=Transgrnaular
IG=Intergranular

Table II

Elastic Moduli for C.C. B-1900+Hf and D.S. Mar-M200+Hf

	Elastic Modulus (psi x10^6)					
	D.S. Mar-M200+Hf (orientation θ)					C.C. B-1900+Hf
Temperature	0°	15°	30°	45°	90°	--
800°F	17	20	26	34	20	25.4
1500°F	14	17	23	30	17	22.2
1700°F	12	15	20	26	16	20.8
1900°F	11.5	13	18	23	12.5	19.4

Summary

Thermal-mechanical fatigue tests have been performed on coated and uncoated superalloys to identify the key parameters controlling the thermal fatigue resistance of gas turbine components. It has been established that coatings are preferred crack initiation sites. The initiation of these coating cracks is a function of the coating mechanical properties, the strain-temperature cycle phase relationship, and the thermal strain range (including the thermal expansion mismatch strains generated between the coating and the underlying superalloy). The propagation rates of superalloy substrate cracks are dependent on the strain intensity factor range, the alloy elastic modulus in the principal strain direction, and the strain-temperature cycle phase relationship.

References

1. C. A. Rau, A. E. Gemma, and G. R. Leverant, Fatigue at Elevated Temperatures, ASTM STP 520, 1973, p. 168.

2. A. E. Gemma, B. S. Langer, and G. R. Leverant, ASTM Symposium on Thermal Fatigue, New Orleans, November 1975, to be published in ASTM STP.

3. S. W. Hopkins, ASTM Symposium on Thermal Fatigue, New Orleans, November 1975, to be published in ASTM STP.

4. T. E. Strangman, Pratt and Whitney Aircraft, unpublished research.

5. M. Gell, G. R. Leverant, and C. H. Wells, Achievement of High Fatigue Resistance in Metals and Alloys, ASTM STP 467, 1970, p. 113.

6. M. Gell and G. R. Leverant, Fatigue at Elevated Temperatures, ASTM STP 520, 1973, p. 37.

7. D. H. Boone, T. E. Strangman, and L. W. Wilson, J. Vac. Sci. Tech., Vol. 11, 1974, p. 641.

8. E. J. Felten, T. E. Strangman, and N. E. Ulion, Coatings for Directional Eutectics", NASA CR-134735, October 1974.

9. T. E. Strangman and S. W. Hopkins, Ceramic Bulletin, Vol. 55, 1976, p. 304.

10. W. Elber, Eng. Frac. Mech., Vol. 2, 1970, p. 37.

11. A. Yuen, S. W. Hopkins, G. R. Leverant, and C. A. Rau, Met. Trans., Vol. 5, 1974, p. 1833.

12. G. T. Hahn, A. R. Rosenfield, and M. Sarrate, Elastic-Plastic Fracture Mechanics-Part III, AFML-FR-67-143, 1970.